Selective Photoconversion of Carbon Dioxide into Methanol Using Layered Double Hydroxides at 0.40 MPa

Masaya Miyano, Hongwei Zhang, Mao Yoshiba, and Yasuo Izumi*[a]

CO_2 photoconversion is a promising method to reduce atmospheric CO_2 concentrations and mitigate energy problems simultaneously. Among the various efficient and stable semiconductor photocatalysts used for this purpose, layered double hydroxides (LDHs) have attracted attention as catalysts for CO_2 photoconversion into CO and/or methanol. In this study, various LDHs of the formula $[M^{II}_3Ga^{III}(OH)_8]_2A{\cdot}mH_2O$ ($M^{II}=Zn^{II}$, Cu^{II}; $A^{2-}=CO_3^{2-}$, $[Cu(OH)_4]^{2-}$) were synthesized and used for CO_2 photoconversion at a reaction pressure of 0.40 MPa in the presence of H_2 to result in the exclusive production of methanol. Furthermore, the pretreatment of carbonate-type LDHs at 423 K boosted the reaction rates by a factor of 7.5–20. Interestingly, $[Zn_3Ga(OH)_8]_2CO_3{\cdot}mH_2O$ was the only LDH that produced methane primarily by an eight-electron reduction (rather than the production of methanol by a six-electron reduction) at a total formation rate of 2.7 $\mu mol\,h^{-1}\,g_{cat}{}^{-1}$ after it was preheated at 423 K and protected by an Ar atmosphere. Conversely, the methanol photogeneration rates of tetrahydroxycuprate-type LDHs were suppressed to less than 0.1 $\mu mol\,h^{-1}\,g_{cat}{}^{-1}$ at 0.40 MPa. In summary, the contribution of the interlayer reaction space created by the partial removal of water molecules and/or carbonate ions of LDHs was suggested.

Introduction

The photocatalytic conversion of CO_2 into fuels is a method to reduce atmospheric CO_2 concentrations and mitigate energy problems simultaneously.[1,2] A further advantage of this process is the generation of methanol as a product for further transportation and storage. The major products reported for CO_2 photoconversion are methane, CO, the formate ion, and methanol. The selective production of methanol has few precedents, particularly for semiconductor-based photocatalysts.[1,2]

Layered double hydroxides (LDHs) of the formula $[M^{II}_3M^{III}(OH)_8]_2A{\cdot}mH_2O$ ($A^{2-}=CO_3^{2-}$, $[Cu(OH)_4]^{2-}$) produce methanol and CO photocatalytically from CO_2 and H_2,[3] and the combination of Cu^{II} and Ga^{III} ions favors methanol formation.[3,4] The selective formation of methanol was preserved for a Zn–Cu LDH exposed to CO_2 and UV/Vis light (cathode), and a proton-conducting film was used to separate it from a WO_3 moisture photo-oxidation catalyst (anode).[5] The doping of LDHs by Ag or Au nanoparticles and phthalocyanines can boost the visible-light-only photoconversion of CO_2 into methanol and CO effectively.[6,7]

In contrast, Ni-Al LDH; LDHs with $M^{II}=Ni$, Mg, Zn and $M^{III}=Al$, Ga, In; and Zn–Al LDH produced mainly CO,[8–12] whereas Zn–Cu–Al and Ni–Cu–Al LDHs produced methane[13] and formic acid, formaldehyde, and methanol,[14] respectively, from CO_2 in liquid water[8–11,14] or moisture.[12,13] The diffusion of photogenerated electrons to CO_2-derived species in LDHs was monitored by using X-ray absorption fine structure analysis (XAFS) and FTIR spectroscopy;[15] however, the origin of selective methanol production over the Zn–Ga LDH from CO_2 and H_2 is still unclear.

In this study, the photocatalytic conversion of CO_2 over Zn–Ga and Zn–Cu–Ga LDHs was investigated at 0.40 MPa of CO_2 and H_2 (Figure 1). Following the water photo-oxidation step [Eq. (1)], H_2 acted as a reductant for CO_2 photoconversion [Eq. (2)].[3–7,15] The metal ion profile of the cationic layers and the type of interlayer anions were varied, and the mechanism of selective methanol formation is discussed below.

$$2\,H_2O \rightarrow O_2 + 4\,H^+ + 4\,e^- \quad (1)$$

$$CO_2 + 6\,H^+ + 6\,e^- \rightarrow CH_3OH + H_2O \quad (2)$$

Results

Characterization of photocatalysts

The XRD patterns of Zn–Ga–CO_3 and Zn–Cu–Ga–CO_3 LDHs are depicted in Figures 2a and b. The diffraction peaks at $2\theta = 11.7$, 23.5, 34.2, 37.0, 38.8–38.9, 43.3–43.6, 46.4,

[a] M. Miyano, H. Zhang, M. Yoshiba, Dr. Y. Izumi
Department of Chemistry
Graduate School of Science
Chiba University
Yayoi 1–33, Inage-ku, Chiba 263–8522 (Japan)
E-mail: yizumi@faculty.chiba-u.jp
The ORCID identification number(s) for the author(s) of this article can be found under http://dx.doi.org/10.1002/ente.201600578.

This publication is part of a Special Issue on "CO_2 Utilization". To view the complete issue, visit: http://dx.doi.org/10.1002/ente.v5.6

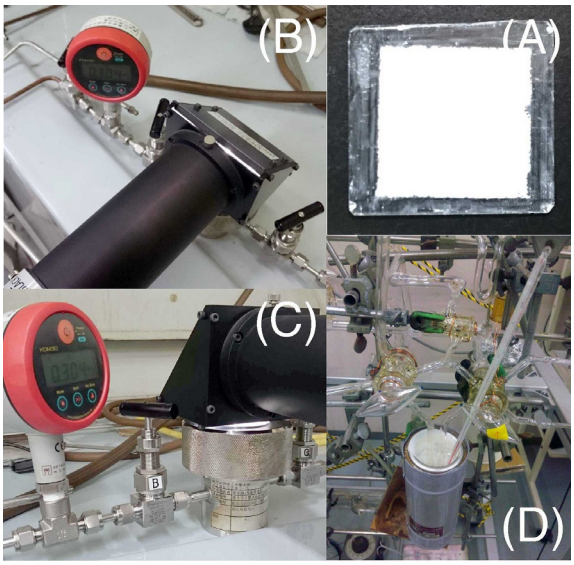

Figure 1. A) Zn–Ga–CO_3 LDH film on a Pyrex glass plate; B) top and C) side views of a high-pressure stainless-steel reactor with quartz windows and a pressure gauge used for CO_2 photoconversion tests under UV/Vis irradiation (500 W Xe arc lamp); D) diethyl ether/dry ice trap (192 K) used to concentrate the produced methanol and water.

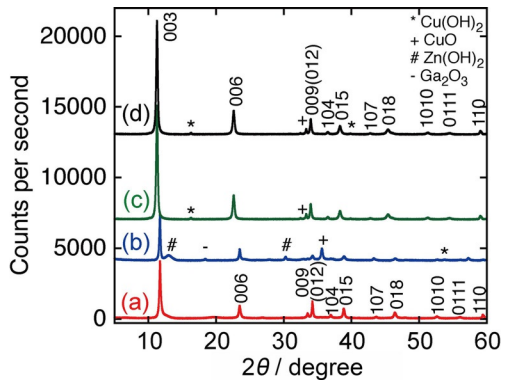

Figure 2. XRD patterns of fresh samples: a) Zn–Ga–CO_3, b) Zn–Cu–Ga–CO_3, c) Zn–Ga–Cu$(OH)_4$, and d) Zn–Cu–Ga–Cu$(OH)_4$.

52.6, 56.0, and 59.4° were assigned to the (003), (006), (009), (104), (015), (107), (018), (1010), (0111), and (110) lattice plane diffractions of the regular layered structure, respectively.[3] The respective interlayer intervals were estimated as 0.756 and 0.757 nm based on the (003) peak (Table 1). These intervals were consistent with the respective values of 0.378×2 and 0.378×2 nm obtained from the diffraction angle of the (006) peak, whereas that of the (009) peak yielded values of 0.262×3 and 0.262×3 nm, respectively. The observed small differences may be because of the overlap of the (009) diffraction peak with that ascribed to the (012) lattice plane and/or because of a minor incompleteness of the LDH crystallites (Figure 2).

The mean thicknesses of the Zn–Ga–CO_3 and Zn–Cu–Ga–CO_3 LDH crystallites were determined as 68 and 75 nm, respectively, based on their (003) peaks [Eq. (3), Experimental Section]. The XRD pattern of Zn–Ga–CO_3 LDH showed no peaks other than those of the LDH crystal structure (Figure 2a); however, peaks of impurities at $2\theta = 13.0$, 18.4, 30.2, 35.6, and 57.3°, ascribed to $Zn(OH)_2$, Ga_2O_3, $Zn(OH)_2$, CuO, and $Cu(OH)_2$ phases, respectively, were observed for Zn–Cu–Ga–CO_3 LDH (Figure 2b).

The XRD patterns measured for as-synthesized Zn–Ga–Cu$(OH)_4$ and Zn–Cu–Ga–Cu$(OH)_4$ are shown in Figure 2c,d. A shift to lower angles (by 0.3–1.6°) was detected for several peaks in the patterns of Zn–Ga–CO_3 and Zn–Cu–Ga–CO_3 to result in peaks at $2\theta = 11.2$, 22.6, 33.9, 36.5, 38.3, 42.8, 45.4, 51.3, 54.4, and 59.1° for Zn–Ga–Cu$(OH)_4$ and Zn–Cu–Ga–Cu$(OH)_4$. These peaks were assigned to the (003), (006), (009), (104), (015), (107), (018), (1010), (0111), and (110) lattice plane diffractions, respectively.[4] The interlayer interval for Zn–Ga–Cu$(OH)_4$ and Zn–Cu–Ga–Cu$(OH)_4$ was determined to be 0.785 nm from their (003) peaks (Table 1).

The mean thickness of the Zn–Ga–Cu$(OH)_4$ and Zn–Cu–Ga–Cu$(OH)_4$ LDH crystallites was 60 and 59 nm, respectively [determined from Eq. (3) and the width of the (003) peak]. In addition to the characteristic LDH diffraction patterns, impurity peaks appeared at $2\theta = 16.3$, 32.5, and 39.8–39.9°, which originate from CuO and $Cu(OH)_2$ impurity phases in both Zn–Ga–Cu$(OH)_4$ and Zn–Cu–Ga–Cu$(OH)_4$ LDHs (Figures 2c and d).

The extrapolation of the absorption edges in the UV/Vis absorption spectra (Figures 3A a–d) yielded x intercepts of $\lambda = 221$, 370, 295, and 428 nm for Zn–Ga–CO_3, Zn–Cu–Ga–CO_3, Zn–Ga–Cu$(OH)_4$, and Zn–Cu–Ga–Cu$(OH)_4$ LDHs, which correspond to band gap (E_g) values of 5.5, 3.4, 4.2, and 2.9 eV, respectively (Table 1). The E_g values of the above samples, calculated from Equation (4) (Experimental Section) by applying different n values, were 5.8–5.4, 3.9–2.7, 5.0–4.0, and 3.6–2.7 eV, respectively (Table 1). In the case of $n = 1/2$ and 3/2, the obtained values were similar to those obtained by simple absorption edge extrapolation (Table 1).

Alternatively, log–log plots of Equation 4 were constructed using E_g values obtained by simple extrapolation (Table 1) to give n values between 0.85 and 1.02. As these values were between 1/2 (allowed direct transition) and 3/2 (forbidden

Table 1. Basic physicochemical properties of the LDH samples used in this study.

Sample	Color	E_g [eV] extrap.[a]	E_g [eV] based on Eq. (4) $n=1/2$	E_g [eV] based on Eq. (4) $n=3/2$	n[b]	Interlayer distance [nm][c]	Crystallite thickness [nm][c]
Zn–Ga–CO_3	white	5.5	5.8	5.4	0.85	0.756	68
Zn–Cu–Ga–CO_3	gray	3.4	3.9	2.7	0.97	0.757	75
Zn–Ga–Cu$(OH)_4$	pale blue	4.2	5.0	4.0	1.02	0.785	60
Zn–Cu–Ga–Cu$(OH)_4$	light blue	2.9	3.6	2.7	0.95	0.785	59
$Zn(OH)_2$	white	3.2	3.2	3.1	1.05		
$Cu(OH)_2$	light blue	2.9	3.0	2.8	0.99		
CuO	black						
Ga_2O_3	white	4.6	4.7	4.5	1.15		

[a] Extrap.: extrapolated value. [b] Obtained from log–log form of Equation (4). [c] Based on (003) peak.

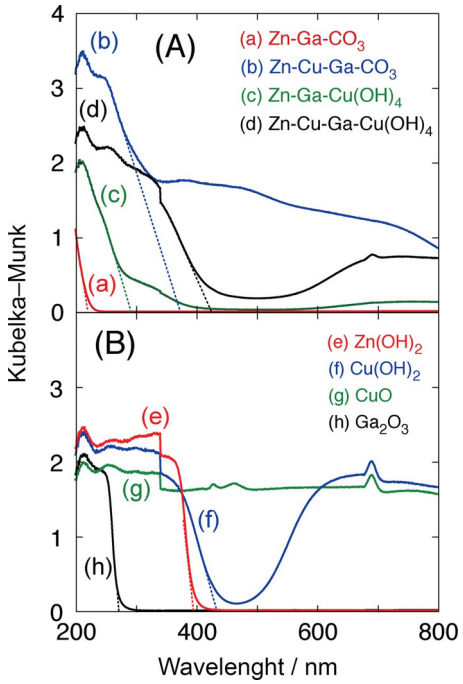

Figure 3. Diffuse reflectance UV/Vis absorption spectra of A) a) fresh Zn–Ga–CO_3, b) Zn–Cu–Ga–CO_3, c) Zn–Ga–Cu$(OH)_4$, and d) Zn–Cu–Ga–Cu$(OH)_4$ and B) e) $Zn(OH)_2$, f) $Cu(OH)_2$, g) CuO, and h) Ga_2O_3 reference samples.

direct transition),[3,16] Zn–Ga–CO_3 could exhibit a direct electronic transition from O 2p to Zn/Ga 4s or 4p levels, and Zn–Cu–Ga–CO_3, Zn–Ga–Cu$(OH)_4$, and Zn–Cu–Ga–Cu$(OH)_4$ could exhibit direct transitions from O 2p to Zn/Ga 4s or 4p levels or Cu 3d, 4s, or 4p levels.

If the interlayer CO_3^{2-} ions of Zn–Ga–CO_3 LDH were replaced with $[Cu(OH)_4]^{2-}$ (which results in Cu/Zn = 1:6 mol/mol), the UV absorption edge shifted to longer wavelengths by 74 nm (Figure 3 A a,c). Accordingly, E_g decreased from 5.5 to 4.2 eV, mostly because of an electronic transition to the Cu 3d level. Additionally, a d–d transition was observed as a weak feature between $\lambda = 560$ and 800 nm (Figure 3 A c).

If half of the Zn^{2+} sites in the cationic layers of Zn–Ga–CO_3 LDH were replaced with Cu^{2+} sites (Cu/Zn = 1:1 mol/mol), the UV absorption edge was further shifted to longer wavelengths by 149 nm (Figures 3 A a and b), and E_g decreased from 5.5 to 3.4 eV, mostly because of electronic transitions to the Cu 3d level. Thus, the amount of Cu was a primary factor to determine the extent of the E_g shift (Figures 2 a–c). In other words, the density of states for Cu 3d in Zn–Cu–Ga–CO_3 was more diffuse than that in Zn–Ga–Cu$(OH)_4$.

Finally, if we replaced both the interlayer and cationic layer sites in Zn–Ga–CO_3 LDH with Cu to produce Zn–Cu–Ga–Cu$(OH)_4$ (Cu/Zn = 4:3 mol/mol) the UV absorption edge shifted to longer wavelengths by 207 nm, and E_g decreased from 5.5 to 2.9 eV, mostly because of electronic transitions to the Cu 3d level at inter- and in-layer sites. The observed decrease (2.6 eV) was greater than that obtained by replacing interlayer sites with $[Cu(OH)_4]^{2-}$ (1.3 eV) or by replacing half of the Zn^{2+} sites in cationic layers (2.1 eV). In accord with the increasing Cu content, the intensity of the d–d transition between $\lambda = 560$ and 800 nm increased in comparison to that observed for Zn–Ga–Cu$(OH)_4$ (Figures 3 A c and d).

Electronic transitions between the O 2p and metal energy levels were observed for reference $Zn(OH)_2$ and Ga_2O_3 samples in the UV region with no absorption detected in the visible region (Figures 3 B e and h). Consistently, these samples were white (Table 1). In contrast, the reference CuO sample was black and absorbed in the whole UV/Vis region (Figure 3 B g). Thus, the gray color (Table 1) and broad absorption peak between $\lambda = 330$ and 800 nm (Figure 3 A b) observed for Zn–Cu–Ga–CO_3 were because of the presence of a CuO impurity, as evidenced by using XRD (Figure 2 b).

The $Cu(OH)_2$ reference material was light blue (Table 1) and its d–d transitions and the absorption edge caused by O 2p to Cu 3d transitions lay in the visible and UV light regions, respectively. $Cu(OH)_2$ exhibits a flat, sheetlike[17] structure that is somewhat similar to that of LDHs. The absorption edge of $Cu(OH)_2$ was extrapolated to $\lambda = 433$ nm (Figure 3 B f), which is shifted significantly to longer wavelengths in comparison to those of Zn–Cu–Ga–CO_3 and Zn–Ga–Cu$(OH)_4$ (Figures 3 A b and c and Table 1). Therefore, the weak shoulders at $\lambda = 310$–330 and 300–400 nm observed for Zn–Cu–Ga–CO_3 and Zn–Ga–Cu$(OH)_4$ (Figures 3 A b and c), respectively, can be ascribed to a $Cu(OH)_2$ impurity. However, the concentrations of this impurity are very low, as estimated from the XRD peak intensity of $Cu(OH)_2$ (Figures 2 b–d). Accordingly, the contribution of this impurity to the d–d transition is marginal (Figures 3 A c and d).

Based on Equation (4), E_g values of 2.9–4.6 eV were determined for $Zn(OH)_2$, $Cu(OH)_2$, and Ga_2O_3, for which n values between 1/2 and 3/2 demonstrated direct O-to-metal electronic transitions (Table 1).

The replacement of CO_3^{2-} with $[Cu(OH)_4]^{2-}$ was confirmed by the dramatic intensity decrease observed by using FTIR spectroscopy for symmetric and antisymmetric stretches of CO_3^{2-}.[15] The Cu/Zn molar ratios of Zn–Cu–Ga–CO_3, Zn–Ga–Cu$(OH)_4$, and Zn–Cu–Ga–Cu$(OH)_4$ (1:1, 1:6, and 4:3, respectively) were confirmed by using X-ray absorption spectroscopy. Interestingly, the octahedral coordination of Cu^{2+} and O atoms was common in these LDHs, as observed by using X-ray absorption near-edge and extended X-ray absorption fine structure spectroscopy. Cu exhibited $Cu(OH)_6$ motifs in the cationic layers of Zn–Cu–Ga–CO_3 and Zn–Cu–Ga–Cu$(OH)_4$, whereas $(\mu\text{-O})_n Cu(OH)_{4-n}(H_2O)_2$ ($n = 1$, 2, or 3; μ-O from the cationic layer; H_2O from interlayer water) units were present in the interlayer sites of Zn–Ga–Cu$(OH)_4$ and Zn–Cu–Ga–Cu$(OH)_4$.[4,15]

The SEM and TEM images of Zn–Ga–CO_3 (Figure 4 A 1 and 6) show flakelike thin layers. The thickness distribution of a single layer (e.g., Figure 4 A 5) centered at 30–40 nm (Figure 4 A, histogram) and the mean value of (42 ± 24) nm were not consistent with the thickness of 68 nm obtained by using XRD (Table 1) as electron-transparent layers were chosen for TEM measurements, which are thinner than those characterized by using XRD. The observed hexagonal crystallites and outlines (perimeters) with thinner contrast are depicted in Figure 4 A 2–4 and the outline (perimeter) width

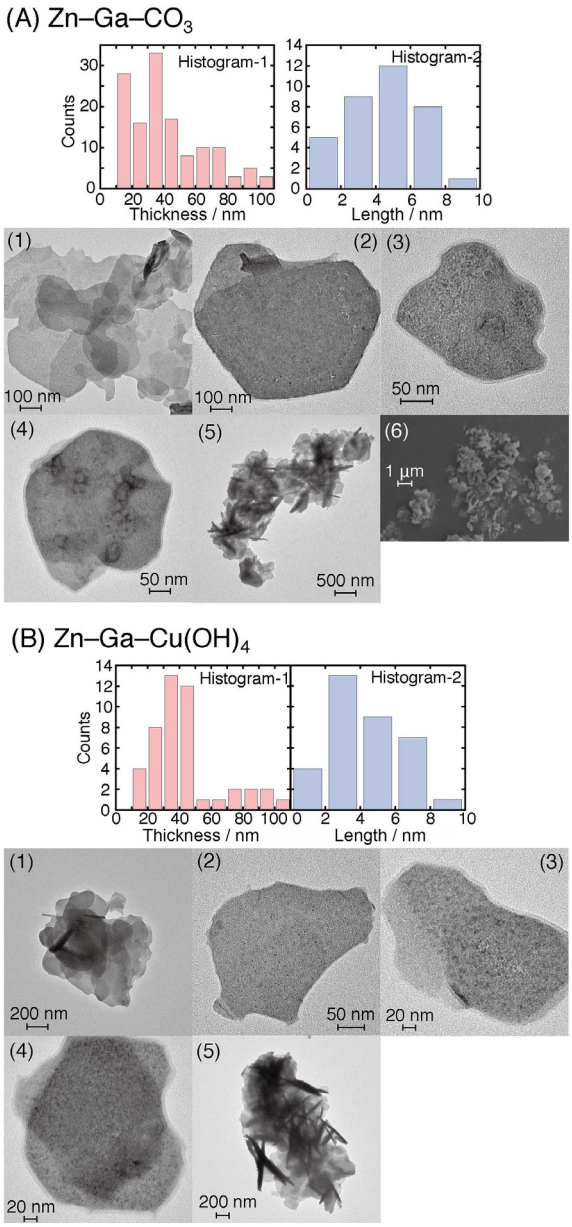

Figure 4. 1–5) TEM and 6) SEM images of fresh A) $Zn–Ga–CO_3$ and B) $Zn–Ga–Cu(OH)_4$. Histograms-1 show the thickness and Histograms-2 the outline (perimeter) length of the flakelike layers.

was centered at 4–6 nm (Figure 4A, histogram). The side face of a single thin layer (thickness ≈ 42 nm) was observed at a nearly parallel angle.

TEM images of $Zn–Ga–Cu(OH)_4$ (Figure 4B) displayed flakelike thin layers (Figure 4B1). The thickness distribution of a single layer (e.g., Figure 4B5) centered at 30–40 nm (Figure 4B, histogram) with a mean of (43 ± 22) nm was fairly consistent with the value of 60 nm determined by using XRD (Table 1). In analogy to the images of $Zn–Ga–CO_3$, outlines (perimeters) of crystallites with a thinner contrast were observed, and the width distribution was centered at 2–4 nm (Figure 4B2–4, histogram).

Photocatalytic tests using LDHs at 0.40 MPa

CO_2 photoconversion tests were performed at a total pressure of 0.40 MPa using four LDH catalysts and H_2. The photocatalyst film formed on a Pyrex plate was dried at 373 K for 12 h and transferred to the high-pressure reactor (Figure 1B and C) under ambient conditions (Table 2A). Methanol was formed as the only the C-containing product, and the observed activity order was: $Zn–Cu–Ga–Cu(OH)_4 > Zn–Ga–CO_3 > Zn–Ga–Cu(OH)_4 > Zn–Cu–Ga–CO_3$.

The selectivity trend at 0.40 MPa contrasted with the results of LDH low-pressure photoconversion tests performed under 2.3 kPa of CO_2+22 kPa of H_2, in which both CO and methanol were obtained as major products (Table 2E1–4).[3,4]

Water was also formed (Table 2A), however, its formation rate was a factor of 780–5500 higher than that of methanol, which demonstrates that it originated exclusively from desorbed interlayer water molecules and was not produced from the reactants. The rates of water formation among LDH photocatalysts varied by a factor of 5.6 (Table 2A), which suggests that the LDH film preheated at 373 K (Figure 1A) absorbed atmospheric moisture into the interlayer space before it was introduced into the reactor (Figure 1C).

Next, LDHs were pretreated at an elevated temperature (423 K) for 12 h to desorb approximately one third of the interlayer water.[3,4] The LDH film on the Pyrex plate was preheated and transferred to the high-pressure reactor under ambient conditions (Table 2B). Again, methanol was observed as the only C-containing product; however, its formation rates were boosted by a factor of 7.5–20 compared to the values obtained for catalysts preheated at 373 K (Table 2A). Apparently, the photoconversion of CO_2 was accelerated by removing some of the interlayer water molecules to liberate reaction space (Scheme 1B).

Water desorption rates (Table 2B) decreased to 56–57% of the values obtained for catalysts preheated at 373 K (Table 2A). Despite this decrease, the partial adsorption of atmospheric moisture during sample transfer from the drying oven held at 423 K to the high-pressure reactor could not be excluded.

To address this issue, a preheated LDH film on a Pyrex plate was transferred to the high-pressure reactor in an atmosphere of Ar to avoid contact with air and thus ensure the partial removal of interlayer water molecules (Table 2C). Except for the $Zn–Ga–CO_3$ photocatalyst, which favored methane production over that of methanol, all LDHs produced methanol exclusively. The total formation rate of C-containing compounds (Σ_C) using $Zn–Ga–CO_3$ LDH was 2.7 $\mu mol\,h^{-1}\,g_{cat}^{-1}$ (Table 2C1). The more effectively liberated interlayer reaction space of the $Zn–Ga–CO_3$ catalyst transferred under Ar favored a further two-electron reduction (Scheme 1C). The catalytic activity based on total C-containing products was in the order: $Zn–Ga–CO_3 \gg Zn–Cu–Ga–CO_3 \gg Zn–Cu–Ga–Cu(OH)_4 \approx Zn–Ga–Cu(OH)_4$.

The total formation rate of C-containing products for $Zn–Ga–CO_3$ transferred under Ar (Table 2C) was higher than

Table 2. Results of CO_2 photoconversion and blank tests at elevated pressure using hydrogen and LDH photocatalysts (10 mg) and rates reported previously.

Entry	Photocatalyst	Reactant [MPa]		Formation rate [$\mu mol\,h^{-1}\,g_{cat}^{-1}$]					
		CO_2	H_2	CO	CH_3OH	CH_4	H_2O	Σ_C[a]	Ref.
A									
1	Zn–Ga–CO_3, 373 K, exposed	0.12	0.28	<0.08	0.040	<0.12	66	0.040	this work
2	Zn–Cu–Ga–CO_3, 373 K, exposed			<0.08	0.011	<0.12	61	0.011	
3	Zn–Ga–Cu$(OH)_4$, 373 K, exposed			<0.08	0.023	<0.12	18	0.023	
4	Zn–Cu–Ga–Cu$(OH)_4$, 373 K, exposed			<0.08	0.087	<0.12	100	0.087	
B									
1	Zn–Ga–CO_3, 423 K, exposed	0.12	0.28	<0.08	0.30	<0.12	37	0.30	
2	Zn–Cu–Ga–CO_3, 423 K, exposed			<0.08	0.22	<0.12	35	0.22	
C									
1	Zn–Ga–CO_3, 423 K, not exposed	0.12	0.28	<0.08	0.049	2.6	13	2.7	
2	Zn–Cu–Ga–CO_3, 423 K, not exposed			<0.08	0.19	<0.12	59	0.19	
3	Zn–Ga–Cu$(OH)_4$, 423 K, not exposed			<0.08	0.028	<0.12	24	0.028	
4	Zn–Cu–Ga–Cu$(OH)_4$, 423 K, not exposed			<0.08	0.034	<0.12	41	0.034	
C′ [b]									
1	Zn–Ga–CO_3, 423 K, not exposed	0.12	0.28	<0.08	0.020	<0.12	9.1	0.020	
D									
5	Zn$(OH)_2$, 423 K, not exposed	0.12	0.28	<0.08	0.048	<0.12	10	0.048	
6	Cu$(OH)_2$, 423 K, not exposed			7.3	0.45	<0.12	34	7.8	
7	CuO, 423 K, not exposed			<0.08	0.14	<0.12	26	0.14	
8	Ga_2O_3, 423 K, not exposed			<0.08	0.059	<0.12	19	0.059	
E									
1	Zn–Ga–CO_3, 290 K, evacuated	0.002 3	0.022	0.080	0.051			0.13	[3]
2	Zn–Cu–Ga–CO_3, 290 K, evacuated			0.079	0.17			0.25	
3	Zn–Ga–Cu$(OH)_4$, 290 K, evacuated			0.13	0.30			0.43	[4]
4	Zn–Cu–Ga–Cu$(OH)_4$, 290 K, evacuated			0.070	0.49			0.56	
1′	Ag/Zn–Ga–CO_3 373 K, exposed	0.12	0.28	0.95	0.10	2.1	5.3	3.2	[20]
9	TiO_2			<0.08	0.027	4.0	56	4.0	
10	g-C_3N_4			<0.08	<0.004	3.8	4.1	3.8	
11	BiOCl			1.9	<0.004	1.1	37	3.0	

[a] Total formation rates of C-containing products. [b] In the absence of UV/Vis light at 303 K.

that obtained for the same catalyst transferred in air by a factor of 9.0 (Table 2B), which indicates that sample transfer under Ar preserved the interlayer reaction space of this LDH liberated by heating at 423 K.

However, the rate of exclusive methanol formation for Zn–Cu–Ga–CO_3 transferred in air was similar to that of the photocatalyst transferred in Ar (Table 2B, C). The exclusive methanol formation rates for Zn–Ga–Cu$(OH)_4$ and Zn–Cu–Ga–Cu$(OH)_4$ preheated at 373 K were almost unchanged if these photocatalysts were preheated at 423 K and transferred under Ar (Table 2A,C). The reason behind these unimproved CO_2 photoconversion rates is not known; however, two plausible reasons can be used to explain this observation: (1) the amount of water in the tests listed in Table 2A and B was not controlled well and was similar to that in the tests summarized in Table 2C and/or (2) the interlayer space of these LDHs was not utilized effectively for catalysis as the major active sites are located only on the outer surface (Scheme 1B).

The results of a blank test using Zn–Ga–CO_3 in the dark at 303 K are shown in Table 2C′. No CO and methane were detected; however, methanol was formed at a rate of 0.020 $\mu mol\,h^{-1}\,g_{cat}^{-1}$. Thus, some methanol is formed thermally rather than photocatalytically if the catalyst activity is relatively low (Table 2A1–3, C3–4). In contrast, the thermal route is negligible for the entries in Table 2A4, B1–2, and C1–2, mainly because of the effect of the liberated LDH interlayer space.

The effects of Zn$(OH)_2$, Cu$(OH)_2$, CuO, and Ga_2O_3 impurities in Zn–Cu–Ga–CO_3 (Figure 2b) and Cu$(OH)_2$ and CuO in Zn–Ga–Cu$(OH)_4$ and Zn–Cu–Ga–Cu$(OH)_4$ (Figures 2c and d) were evaluated. In photocatalytic tests under 0.40 MPa of CO_2+H_2, the total formation rates of C-containing compounds for Zn$(OH)_2$ and Ga_2O_3 were low (0.048–0.059 $\mu mol\,h^{-1}\,g_{cat}^{-1}$, Table 2D5 and 8), which indicates that the contribution of these impurities on the performance of Zn–Cu–Ga–CO_3 (Table 2C2) was negligible.

In contrast, CuO photoconverted CO_2 into methanol at a moderate rate (0.14 $\mu mol\,h^{-1}\,g_{cat}^{-1}$; Table 2D7), which shows that a low concentration of this impurity may contribute to the lower rates observed for Zn–Ga–Cu$(OH)_4$ and Zn–Cu–Ga–Cu$(OH)_4$ (0.028–0.034 $\mu mol\,h^{-1}\,g_{cat}^{-1}$; Table 2C3 and 4). As the photocatalytic performances of Zn–Cu–Ga–CO_3 and CuO were similar (Table 2C2 and D7), the contribution of the CuO impurity to the rates observed for Zn–Cu–Ga–CO_3 is marginal because of its low concentration.

Surprisingly, the photoconversion of CO_2 over Cu$(OH)_2$ produced CO and methanol as the major and minor products, respectively, at a total formation rate of 7.8 $\mu mol\,h^{-1}\,g_{cat}^{-1}$ (Table 2D6). As no CO formation was ob-

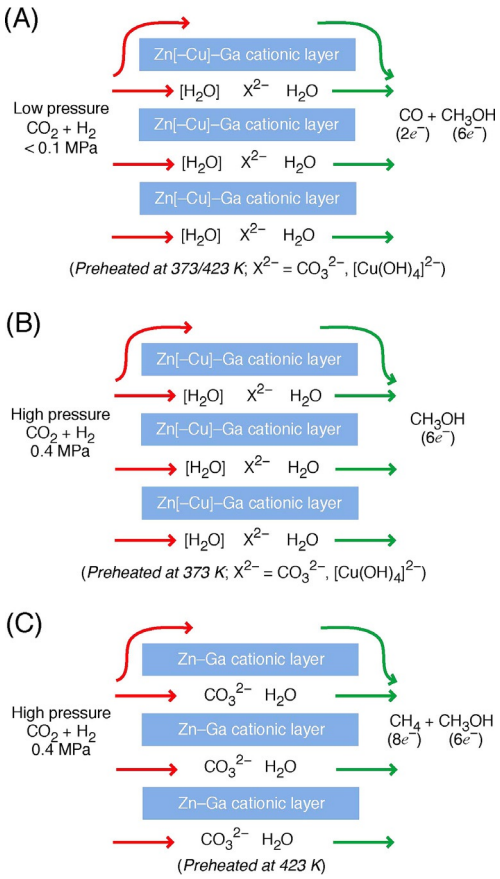

Scheme 1. Reaction space and products of CO_2 photoconversion at A) low pressure for LDHs pretreated at 373 K, B) high pressure for LDHs pretreated at 373 K, and C) high pressure for LDHs pretreated at 423 K.

served for the LDHs studied, the effect of the $Cu(OH)_2$ impurity can be excluded. Only the reference catalyst $Cu(OH)_2$ was active because of the partial decomposition of bulk $Cu(OH)_2$ to CuO during pretreatment at 423 K, and the resulting mixture of $Cu(OH)_2$ and CuO phases is advantageous for CO_2 photoconversion.

Discussion

Carbonate-type Zn–Ga and Zn–Cu–Ga LDHs and their tetrahydroxycuprate-type counterparts were synthesized and their high purity was confirmed by using XRD and UV/Vis spectroscopy (Figures 2 and 3). Traces of impurities such as $Zn(OH)_2$, Ga_2O_3, CuO, and $Cu(OH)_2$ were detected; however, their amounts were lower than those in materials prepared previously[3,4] because of the slow crystallization during drying on a wide Pyrex plate for five days. Notably, no impurities were detected in the most active Zn–Ga–CO_3 catalyst in this study, and these impurities were shown to be inert at a reactant pressure of less than 0.10 MPa.[3,4]

In this study, $Zn(OH)_2$ and Ga_2O_3 impurities were inactive at a reactant pressure of 0.40 MPa (Table 2 D 5, 8) and did not contribute to the rates observed for Zn–Cu–Ga–CO_3 (Figure 2 b and Table 2 C 2). CuO exhibited a moderate activity toward methanol production (Table 2 D 7), which possibly affected the results of poorly performing Zn–Ga–$Cu(OH)_4$ and Zn–Cu–Ga–$Cu(OH)_4$ but had a negligible influence on Zn–Cu–Ga–CO_3 if we take the concentration of this impurity into account (Figures 2 b–d). Bulk $Cu(OH)_2$ is probably activated by heating at 423 K to produce an interface between $Cu(OH)_2$ and CuO for the selective formation of CO (Table 2 D 6). Such effective CO_2 photoconversion sites were not formed in the LDHs studied herein, and no CO was produced (Table 2 A–C).

The salient point of CO_2 photoconversion at 0.40 MPa (0.12 MPa of CO_2 and 0.28 MPa of H_2) is the exclusive selectivity toward methanol, whereas both CO and methanol were produced over these LDHs at 24 kPa (2.3 kPa of CO_2 and 22 kPa of H_2; Scheme 1 A). Thus, above 0.40 MPa, the higher concentrations of reactants and/or intermediates in the reaction space of the LDHs facilitate the sequential six-electron reduction of CO_2 to methanol (Scheme 1 B) rather than its two-electron reduction to CO.

For CO_2 photoconversion at 0.40 MPa, the catalyst activity depended critically on the pretreatment conditions of carbonate-type LDHs (Table 2 A 1, 2 A 2, 2 B 1, 2 B 2, 2 C 1, and 2 C 2), and the methanol formation rates increased by a factor of 7.5–20 as the pretreatment temperature increased from 373 to 423 K (Table 2 A and B). In the special case of Zn–Ga–CO_3, the sample heated at 423 K and transferred to the high-pressure reactor under Ar (Table 2 C) produced methane (eight-electron reduction) rather than methanol (six-electron reduction). The total formation rate of C-containing products reached 2.7 $\mu mol\,h^{-1}\,g_{cat}{}^{-1}$, which corresponds to a 9.0-fold increase compared to that observed for the same catalyst transferred in air (Table 2 B 1 and C 1). This change can be understood by assuming a subsequent two-electron reduction path favored by the more efficient and open interlayer reaction space in the tests listed in Table 2 C (Scheme 1 C). Exclusive methane formation from CO_2 and moisture has been reported for Zn-Ce and Zn-Ti LDHs irradiated by UV light ($\lambda = 185$ nm).[18]

In clear contrast, the rates of methanol formation for tetrahydroxycuprate-type LDHs were suppressed to less than 0.1 $\mu mol\,h^{-1}\,g_{cat}{}^{-1}$ at 0.40 MPa (Table 2 A 3, 2 A 4, 2 C 3, and 2 C 4). The interlayer reaction space[19] created by the partial removal of water molecules and/or carbonate ions of LDHs is believed to be important for CO_2 photoconversion.

For Zn–Ga–CO_3, the rate of water formation decreased progressively with the improvement of the pretreatment conditions (Table 2 A→B→C) and the CO_2 photoconversion rate increased concomitantly. In the case of Zn–Cu–Ga–CO_3, the water formation rate did not decrease simply because of the improved pretreatment conditions; however, the extent of this decrease correlated well with the CO_2 photoconversion rate (Table 2 A 2, B 2, and C 2). In comparison to Zn–Ga–CO_3, Zn–Cu–Ga–CO_3 was destabilized by the inclusion of $3d^9$ Cu^{2+} ions in the cationic layer because of the Jahn–Teller effect,[3] and the desorption of interlayer water before/during photocatalytic tests for 5 h was relatively difficult to reproduce quantitatively.

The formation rates of C-containing products listed for Zn–Ga–CO_3 and Zn–Cu–Ga–CO_3 in Table 2 B–C (0.40 MPa) are comparable to those obtained at 24 kPa (Table 2 E 1–4), except for the higher value of 2.7 $\mu mol\,h^{-1}\,g_{cat}^{-1}$ (Table 2 C 1). The rates observed for Zn–Ga–Cu$(OH)_4$ and Zn–Cu–Ga–Cu$(OH)_4$ (Table 2 A and C, 0.40 MPa) were one order of magnitude lower than those obtained at 24 kPa (Table 2 E 1–4). Thus, the reaction order was zero or even negative for most of the LDHs used in this study except for Zn–Ga–CO_3 in contrast to the reported TiO_2, g-C_3N_4, and BiOCl photocatalysts until 0.40 MPa,[20] presumably because of the strong adsorption of reactants/intermediates in the interlayer reaction space of LDHs.

The photoconversion of CO_2 at 0.40 MPa over Ag-doped Zn–Ga–CO_3 was reported to produce methane, CO, and minor amounts of methanol at a total formation rate of 3.2 $\mu mol\,h^{-1}\,g_{cat}^{-1}$ (Table 2 E 1′)[20] and a similar value was observed for Ag-free Zn–Ga–CO_3 (2.7 $\mu mol\,h^{-1}\,g_{cat}^{-1}$; Table 2 C 1) by pretreatment at 423 K and sample transfer under Ar. The performance of Zn–Ga–CO_3 at 0.40 MPa (Table 2 C 1) was equivalent to that of BiOCl (Table 2 E 11) and close to that of TiO_2 and g-C_3N_4 (Table 2 E 9 and 10). Thus, the doping of LDHs with effective electron-trapping and/or surface plasmon resonance sites and the optimization of the pretreatment/transfer conditions (Table 2 C) is expected to further improve the catalytic performance of CO_2 and H_2 at 0.40 MPa.

Conclusions

The photoconversion of CO_2 was studied for various layered double hydroxides (LDHs). With H_2 as a reductant, methanol production over the LDHs was achieved at less than 0.1 MPa and became exclusive at 0.40 MPa. The CO_2 photoconversion rates observed for carbonate-type LDHs Zn–Ga–CO_3 and Zn–Cu–Ga–CO_3 were improved by increasing the pretreatment temperature from 373 to 423 K (0.19–2.7 $\mu mol\,h^{-1}\,g_{cat}^{-1}$), which suggests the liberation of the interlayer reaction space by the removal of approximately one third of the interlayer water molecules. For Zn–Ga–CO_3 heated at 423 K and transferred to the reactor under Ar, methane was formed selectively rather than methanol, which suggests that the liberation of further interlayer sites enabled the eight-electron reduction of CO_2 to methane. In contrast, tetrahydroxycuprate-type LDHs Zn–Ga–Cu$(OH)_4$ and Zn–Cu–Ga–Cu$(OH)_4$ showed suppressed rates of 0.023–0.087 $\mu mol\,h^{-1}\,g_{cat}^{-1}$, probably because only the outer surface[21] contributed to CO_2 photoconversion for this type of LDH.

Experimental Section

Synthesis of LDH photocatalysts

Two carbonate-type LDHs $[Zn_3Ga(OH)_8]_2CO_3{\cdot}m\,H_2O$ and $[Zn_{1.5}Cu_{1.5}Ga(OH)_8]_2CO_3{\cdot}m\,H_2O$ were synthesized according to procedures reported previously.[3] An aqueous solution (20 mL) of 0.75 M $Zn(NO_3)_2{\cdot}6\,H_2O$ (>99.9%, Wako Pure Chemical) and 0.25 M $Ga(NO_3)_3{\cdot}n\,H_2O$ (n=7–9, >99.9%, Wako Pure Chemical) or 0.375 M $Zn(NO_3)_2{\cdot}6\,H_2O$, 0.375 M $Cu(NO_3)_2{\cdot}3\,H_2O$ (>99.9%, Wako Pure Chemical), and 0.25 M $Ga(NO_3)_3{\cdot}n\,H_2O$ was dropwise added to a 0.075 M sodium carbonate (>99.8%, Wako Pure Chemical) aqueous solution (100 mL) at a rate of 0.24 mL min^{-1} at 290 K under stirring at 900 rpm. The mixture was stirred at 290 K for 2 h, and the solution pH was adjusted to 8 by adding 1.0 M NaOH (≈30 mL total; >93%, Wako Pure Chemical). Subsequently, the temperature was increased to 353 K, and the reaction solution was stirred for 22 h. The obtained precipitates were filtered through a polytetrafluoroethene membrane filter (Omnipore JVWP04700) with a pore size of 0.1 μm and washed with deionized water. In the drying step after the final washing step, a very thin intermediate product layer on a flat wide-area Pyrex glass plate was produced in a glovebox over 5 days to improve the purity of the crystalline LDHs. The produced LDHs were denoted as Zn–Ga–CO_3 and Zn–Cu–Ga–CO_3, respectively, in which m was generally equal to half of the total amount of metal cations.

Two tetrahydroxycuprate-type LDHs $[Zn_3Ga(OH)_8]_2[Cu(OH)_4]{\cdot}m\,H_2O$ and $[Zn_{1.5}Cu_{1.5}Ga(OH)_8]_2[Cu(OH)_4]{\cdot}m\,H_2O$ were synthesized according to procedures described previously.[4] An aqueous solution (20 mL) of 0.75 M $Zn(NO_3)_2{\cdot}6\,H_2O$ and 0.25 M $Ga(NO_3)_3{\cdot}n\,H_2O$ or 0.375 M $Zn(NO_3)_2{\cdot}6\,H_2O$, 0.375 M $Cu(NO_3)_2{\cdot}3\,H_2O$, and 0.25 M $Ga(NO_3)_3{\cdot}n\,H_2O$ was dropwise added to a 0.025 M aqueous solution (100 mL) of $(NH_4)_2CuCl_4{\cdot}2\,H_2O$ (>98%, Wako Pure Chemical) at a rate of 0.32 mL min^{-1} at 290 K under stirring at 900 rpm. The mixture was stirred at 290 K for 2 h, and the solution pH was adjusted to 8 by adding 1.0 M NaOH (≈44 mL total). Subsequently, the temperature was increased to 353 K, and the reaction solution was stirred for 22 h. The obtained precipitates were filtered through a JVWP04700 filter and washed with deionized water. In the drying step after the final washing step, a very thin intermediate product layer on a flat wide-area Pyrex glass plate was produced in a glovebox over 5 days to improve the purity of crystalline LDHs. The produced LDHs were denoted as Zn–Ga–Cu$(OH)_4$ and Zn–Cu–Ga–Cu$(OH)_4$, respectively. Notably, the interlayer $[Cu(OH)_4]^{2-}$ reacted with the hydroxy groups of the cationic layer in a dehydration reaction to result in Cu ion coordination by oxo and hydroxy groups, similar to the coordination environment of Cu^{2+} in the cationic layer.[4,15]

$Zn(OH)_2$ was synthesized according to a procedure reported previously[22] from ZnO (1.0 g; >99%; Wako Pure Chemical) and 20 wt% aqueous NaOH (20 mL). Cu$(OH)_2$ (>90%, Wako Pure Chemical), CuO (>99.9%, Wako Pure Chemical), and Ga_2O_3 (>99.99%, Wako Pure Chemical) were used as received. The light-blue color of the as-received Cu$(OH)_2$ turned to dark brown at 423 K during the preparation of the photocatalyst film, which indicates its (partial) transformation into CuO.

Characterization

XRD patterns were recorded by using a diffractometer (model D8 ADVANCE, Bruker) at the Center for Analytical Instrumentation, Chiba University, at 2θ=5.0–60° with a scan step of 0.01° and a scan rate of 5 s $step^{-1}$. Measurements were performed at 40 kV and 40 mA using CuK_α emission (λ=0.15419 nm)[23] and a Ni filter. Crystallite sizes (t) were estimated using the Scherrer equation [Eq. (3)]:

$$t = \frac{0.9\lambda}{(\text{Full width at half maximum}) \times cos\theta_B} \quad (3)$$

UV/Vis spectra were recorded by using a model V-650 (JASCO) spectrophotometer equipped with an integrating sphere (ISV-469, JASCO) for diffuse reflectance measurements at 200–800 nm. The E_g values were estimated by a simple extrapolation of the absorption edge or by fitting to the Davis–Mott equation [Eq. (4)]:

$$\alpha h\nu \propto (h\nu - E_g)^n \quad (4)$$

in which α, h, and ν are the absorption coefficient, Planck's constant, and the frequency of light, respectively, and n is 1/2, 3/2, 2, or 3 for allowed direct, forbidden direct, allowed indirect, and forbidden indirect electronic transitions, respectively.[3,16]

SEM imaging was performed by using a JSM-6510A instrument (JEOL) at the Center for Analytical Instrumentation, Chiba University. A W filament was used in the electron gun, and the electron accelerating voltage was 3.0 kV. Au particles were coated by using a JFC-1100 instrument (JEOL). The employed magnification was 10 000–20 000×.

TEM imaging was performed by using a model H-7650 transmission electron microscope (Hitachi) at an accelerating voltage of 100 kV. The samples were mounted on a carbon-coated Cu grid mesh (150 mesh per inch) coated with a copolymer film of polyvinyl alcohol and formaldehyde (Formvar, Monsanto). A W filament was used in the electron gun. The employed magnification was 6000–100 000×.

CO_2 photoconversion tests

LDH catalysts were immersed in deionized water ($<0.055\ \mu S\,cm^{-1}$) produced by using an RFU424TA water purification system (Advantec) and agitated by ultrasound (430 W, 38 kHz) for 3 min. The suspension was cast on a Pyrex glass plate (25 mm × 25 mm × 1 mm) and dried for 12 h at 373 or 423 K. The mass and area of the obtained films was 10 mg and 20 mm × 20 mm, and their thickness was ≈12 μm (Figure 1A). These films were introduced into a homemade high-pressure stainless-steel reactor with quartz double windows, a pressure gauge, and Swagelok valves (Figures 1B, C) for photoconversion tests. The effective internal volume of the reactor was 98.4 mL.

Subsequently, 0.40 MPa of a CO_2/H_2 mixture (3:7 v/v) was introduced into the reactor. The photocatalyst (Table 1) was irradiated by UV/Vis light emitted by a 500 W Xe arc lamp (model OPM2-502, Ushio) through quartz windows in the reactor chamber for 5 h (Figure 1C). The distance between the light exit point and the photocatalyst surface was 82.7 mm. Light transmission was checked by using a photosensor and a counter (model PCM-01, Prede; and model KADEC-UP, North One, respectively). The light intensity at the center of the photocatalyst was $90.2\ mW\,cm^{-2}$. The quartz windows of the high-pressure reactor absorbed/reflected/diffracted 9.5% of incident light, whereas 10 mg of our standard photocatalyst film (Pd/TiO_2) on the Pyrex glass plate absorbed/reflected/diffracted 49% of incident light.

After 5 h of irradiation, the gas mixture was analyzed by using columns packed with 13X-S molecular sieves and polyethylene glycol (PEG-6000) supported on Flusin P (GL Sciences) set in a GC equipped with a thermal conductivity detector (model GC-8A, Shimadzu).[3–5,15] He (>99.999 95%) was used as a carrier gas. The amounts of produced methanol and moisture were checked by concentrating them in a trap cooled by a mixture of diethyl ether and dry ice (192 K) to achieve separation from H_2 and most of the CO_2 (Figure 1D).

Typically, the initial pressure of 0.400 MPa at 295 K increased gradually to 0.407 MPa in approximately 10 min during the CO_2 photoconversion tests. As the critical pressures of H_2 and CO_2 are relatively high (1.30 and 7.38 MPa, respectively), the reaction gas in this study (0.28 MPa H_2, 0.12 MPa CO_2) can be approximated to be an ideal gas. Therefore, the temperature of the reaction gas reached 300 K. We confirmed that the external surface of the high-pressure reactor (Figure 1C) reached the same temperature, which is in thermal equilibrium with the reaction gas.

The thin photocatalyst film (10 mg) on Pyrex glass and the reactor were in contact during photocatalytic tests. Even if we assume that the catalyst film retained all the heat of methanol or methane formation (15 and 130 nmol maximum), the maximum temperature increase is calculated as 0.10 and 2.9 K, respectively, based on Equations (5) and (6), with the catalyst heat capacity approximated to that of $Zn(OH)_2$ ($72.4\ J\,mol^{-1}\,K^{-1}$). Thus, we chose 303 K as a blank test temperature for LDH photocatalysts under 0.40 MPa of CO_2+H_2 (Table 2C′).

$$CO_2 + 3\,H_2 \rightarrow CH_3OH + H_2O,\ \Delta H_r^\circ = -50\ kJ\,mol^{-1} \quad (5)$$

$$CO_2 + 4\,H_2 \rightarrow CH_4 + 2\,H_2O,\ \Delta H_r^\circ = -165\ kJ\,mol^{-1} \quad (6)$$

Acknowledgements

The authors acknowledge financial support from the Grant-in-Aid for Scientific Research C (26410204, 22550117) provided by the Japan Society for the Promotion of Science and the Leading Research Promotion Program (2015) of the Institute for Global Prominent Research, Chiba University.

Keywords: copper · layered double hydroxides · photochemistry · reduction · zinc

[1] Y. Izumi, *Coord. Chem. Rev.* **2013**, *257*, 171–186.
[2] Y. Izumi in *Advances in CO_2 Capture, Sequestration, and Conversion Vol. 1194* (Eds.: F. Jin, L.-N. He, Y. H. Hu), ACS Books, Washington DC, **2015**, pp. 1–46.
[3] N. Ahmed, Y. Shibata, T. Taniguchi, Y. Izumi, *J. Catal.* **2011**, *279*, 123–135.
[4] N. Ahmed, M. Morikawa, Y. Izumi, *Catal. Today* **2012**, *185*, 263–269.
[5] M. Morikawa, Y. Ogura, N. Ahmed, S. Kawamura, G. Mikami, S. Okamoto, Y. Izumi, *Catal. Sci. Technol.* **2014**, *4*, 1644–1651.
[6] S. Kawamura, M. C. Puscasu, Y. Yoshida, Y. Izumi, G. Carja, *Appl. Catal. A* **2015**, *504*, 238–247.
[7] S. Kawamura, N. Ahmed, G. Carja, Y. Izumi, *Oil Gas Sci. Technol.* **2015**, *70*, 841–852.
[8] S. Iguchi, K. Teramura, S. Hosokawa, T. Tanaka, *Appl. Catal. A* **2016**, *521*, 160–167.
[9] S. Iguchi, S. Kikkawa, K. Teramura, S. Hosokawa, T. Tanaka, *Phys. Chem. Chem. Phys.* **2016**, *18*, 13811–13819.
[10] S. Iguchi, K. Teramura, S. Hosokawa, T. Tanaka, *Phys. Chem. Chem. Phys.* **2015**, *17*, 17995–18003.

[11] K. Teramura, S. Iguchi, Y. Mizuno, T. Shishido, T. Tanaka, *Angew. Chem. Int. Ed.* **2012**, *51*, 8008–8011; *Angew. Chem.* **2012**, *124*, 8132–8135.
[12] Y. Zhao, G. Chen, T. Bian, C. Zhou, G. I. N. Waterhouse, L.-Z. Wu, C.-H. Tung, L. J. Smith, D. O'Hare, T. Zhang, *Adv. Mater.* **2015**, *27*, 7824–7831.
[13] Q. Guo, Q. Zhang, H. Wang, Z. Liu, Z. Zhao, *Catal. Commun.* **2016**, *77*, 118–122.
[14] M. Lv, H. Liu, *J. Solid State Chem.* **2015**, *227*, 232–238.
[15] M. Morikawa, N. Ahmed, Y. Yoshida, Y. Izumi, *Appl. Catal. B* **2014**, *144*, 561–569.
[16] F. Wooten, *Optical Properties of Solids*, Academic Press, New York, 1972, p. 14.
[17] S. Sun, Y. Sun, A. Chen, X. Zhang, Z. Yang, *Analyst* **2015**, *140*, 5205–5215.
[18] F. Sastre, A. Corma, H. Garcia, *J. Am. Chem. Soc.* **2012**, *134*, 14137–14141.
[19] K. A. D. de Freitas Castro, F. Wypych, A. Antonangelo, K. M. Mantovani, A. Bali, G. M. Ucoski, K. J. Ciuffi, T. E. Cintra, *J. Colloid Interface Sci.* **2016**, *478*, 374–383.
[20] S. Kawamura, H. Zhang, M. Tamba, T. Kojima, M. Miyano, Y. Yoshida, M. Yoshiba, Y. Izumi, *J. Catal.* **2017**, *345*, 39–52.
[21] M. B. J. Roeffaers, B. F. Sels, H. Uji-i, F. C. De Schryver, P. A. Jacobs, D. E. De Vos, J. Hofkens, *Nature* **2006**, *439*, 572–575.
[22] O. K. Srivastava, E. A. Secco, *Canadian J. Chem.* **1967**, *45*, 579–583.
[23] G. Zschornack, *Handbook of X-ray Data*, Springer, Berlin/Heidelberg **2007**, p. 233.

Manuscript received: September 15, 2016
Revised manuscript received: November 27, 2016
Accepted manuscript online: November 29, 2016
Version of record online: February 20, 2017

